Stretchable conductive nanocomposite based on alginate hydrogel and silver nanowires for wearable electronics

Cite as: APL Mater. **7**, 031502 (2019); https://doi.org/10.1063/1.5063657
Submitted: 29 September 2018 . Accepted: 12 November 2018 . Published Online: 20 December 2018

Chanhyuk Lim, Yoonsoo Shin, Jaebong Jung, Ji Hoon Kim, Sangkyu Lee, and Dae-Hyeong Kim

Stretchable conductive nanocomposite based on alginate hydrogel and silver nanowires for wearable electronics

Cite as: APL Mater. 7, 031502 (2019); doi: 10.1063/1.5063657
Submitted: 29 September 2018 • Accepted: 12 November 2018 •
Published Online: 20 December 2018

Chanhyuk Lim,[1,2,a] Yoonsoo Shin,[1,2,a] Jaebong Jung,[3] Ji Hoon Kim,[3] Sangkyu Lee,[1,b] and Dae-Hyeong Kim[1,2,b]

AFFILIATIONS

[1] Center for Nanoparticle Research, Institute for Basic Science (IBS), Seoul 08826, South Korea
[2] School of Chemical and Biological Engineering, Institute of Chemical Process, Seoul National University, Seoul 08826, South Korea
[3] School of Mechanical Engineering, Pusan National University, Busan 46241, South Korea

[a] C. Lim and Y. Shin contributed equally to this work.
[b] Authors to whom correspondence should be addressed: dkim98@snu.ac.kr and sangkyulee@snu.ac.kr

ABSTRACT

Wearable electronic devices are used to perform various electronic functions on the human skin, and their mechanical softness while maintaining high performances is critical. Therefore, there is a need to develop novel materials with outstanding softness and high electrical and ionic conductivity for wearable electronics. Here, we present an intrinsically stretchable and conductive nanocomposite based on alginate hydrogels and silver nanowires (AgNWs). The developed nanocomposite was applied to highly conductive soft electrodes that can be used in various wearable electronic devices. The nanocomposite electrode was prepared by cross-linking alginate molecules in the presence of AgNWs, exhibiting higher electrical, ionic conductivity, higher stretchability, and lower modulus than conventional conducting rubbers. By forming a bilayer structure with the nanocomposite and the ultrasoft hydrogel layer, the mechanical properties of the nanocomposite device could be matched to that of the human skin. We used the nanocomposite electrode for fabricating key device components of wearable electronics, such as a wearable antenna and a skin-mountable supercapacitor. Such demonstrations successfully proved the effectiveness of the proposed nanocomposite as a soft conducting material for wearable electronics.

Conductive hydrogels have been applied to mechanically soft and deformable electrodes in various stretchable devices such as wearable sensors,[1,2] touch panels,[3] and energy storage devices.[4] Although hydrogel itself is generally not conductive, it can be made conductive by adding ionic salts and/or conductive polymers. This conductive hydrogel has many free ions, which play an important role when used as an electrolyte in electrochemical devices. For example, an ionic hydrogel has been applied as a solid electrolyte to fabricate aqueous batteries[5] and supercapacitors.[6] Moreover, hydrogels can be integrated onto conventional metal electrodes to realize a soft contact between the human skin and the electrode in wearable electronics,[7,8] thereby reducing the contact impedance in various bio-sensing applications.[9,10] In addition, hydrogel films can be formed even on hydrophobic films, such as films of silicon rubbers,[11] thus making it easier to apply hydrogel electrodes to wearable devices.[12]

However, the low electrical conductivity of conventional conducting hydrogels limits their application to a wide range of high performance wearable electronic devices. Therefore, many attempts have been made to increase the electrical conductivity of hydrogels by adding electrically conductive filler materials.[13,14] Conductive polymers,[15] such as poly(3,4-ethylenedioxythiophene)-poly(styrenesulfonate) (PEDOT:PSS),

are one of the promising conductive materials that can be used to fabricate electrically conductive hydrogels owing to their electrically conducting and mechanically soft nature.[16,17] Despite many technological advances, however, conductive hydrogels using free ions and/or conductive polymers are not conductive enough particularly in comparison with ultrathin metal/oxide thin films with a stretchable design,[18] conductive rubbers based on metal nanowires,[19] and other carbon based stretchable electrodes,[20,21] which makes them unsuitable for high performance wearable electronic devices.

Meanwhile, metallic materials have extremely high electrical conductivity compared to other conducting materials such as metal oxides, conducting polymers,[22] and carbons.[23] Therefore, the formulation of metal nanomaterials into hydrogels can make highly conductive hydrogel-based nanocomposites. However, the cross-linking of hydrogel monomers or molecules is disturbed by the presence of metal nanomaterials.[24] Various methodologies such as insertion of metal nanoparticles into pre-formed hydrogel[25] and direct synthesis of metal nanoparticles[26] or nanodendrites[27] in the hydrogel matrix have been developed as alternatives. However, 1D metal nanowires uniformly dispersed in a polymer matrix are more favorable for creating a 3D percolation network than other shapes of metal nanomaterials such as nanoparticles.[28] Therefore, a new strategy to fabricate a conductive hydrogel based on 1D metal nanowires is needed.

In this work, the fabrication method, characterization, and device application of a soft conductive nanocomposite using alginate hydrogels and AgNWs are presented. The developed hydrogel-based nanocomposite is applied for highly conductive and stretchable electrodes used in wearable electronics. AgNWs are chosen as a metallic conducting filler material owing to their excellent electrical conductivity, ultralong 1D structure,[29] and facile synthesis on a large scale, which make a good percolation network in the hydrogel matrix. As a polymeric media for the nanocomposite,[30] a tough alginate hydrogel formed by ionic cross-linking between alginate molecules and multivalent cations such as Ca^{2+} is used. As the fabrication process of alginate hydrogels does not involve the formation of covalent bonds by polymerization, it is easy to formulate various kinds of inorganic and metallic nanomaterials to functionalize the hydrogel, and in this study, the AgNWs were added to the alginate hydrogel to help obtain high electrical conductivity. The high electrical conductivity of the hydrogel nanocomposite makes it suitable for device applications that require a large flow of both alternating current and direct current (AC and DC). An ultra-soft layer of poly(acrylamide) (PAAm) hydrogel is attached underneath the nanocomposite electrode as a stress-releasing layer, thereby matching the mechanical property of the nanocomposite electrode to that of the human skin.[31] Using the nanocomposite electrode based on the bilayer structure of the nanocomposite and hydrogel substrate, wearable devices such as a skin-mountable antenna and a supercapacitor were successfully demonstrated.

The alginate hydrogel-based nanocomposite was prepared using a drying process [Fig. 1(a)]. First, 2% sodium alginate was dissolved in an aqueous suspension of AgNWs (0.5 wt. %, DUKSAN Hi-Metal Co., Korea) with stirring at 70 °C. Then the mixture solution was poured onto a Petri dish and dried at 40 °C. The dried alginate-AgNW nanocomposite film was treated with 0.1M $CaCl_2$ aqueous solution for 20 min for cross-linking between functional groups of alginate chains. The presence of the AgNWs in the alginate molecules does not disturb the ionic cross-linking between the alginate molecules and Ca^{2+} [Fig. 1(b)]. Finally, the Ca^{2+}-treated nanocomposite film was washed with distilled water and patterned into various forms of composite electrodes using a laser cutting process [Fig. 1(b)].

The alginate hydrogel was used as the hydrogel matrix for the nanocomposite instead of the frequently used PAAm hydrogels.[32] The PAAm hydrogels are typically prepared using free radical polymerization, and a clear hydrogel film is obtained on a glass [Fig. 1(c), left]. However, the addition of AgNWs to the precursor solution of the PAAm hydrogel hindered its polymerization, causing inhomogeneity of the nanocomposite film [Fig. 1(c), right]. The resulting PAAm hydrogel remained as a mixture of the hydrogel and pre-cured solution (movie of the supplementary material). By contrast, in the case of the alginate hydrogel, the homogeneous hydrogel-based nanocomposite films are effectively prepared regardless of the presence of AgNWs [Fig. 1(d)]. The developed nanocomposite film exhibits the lowest resistance (i.e., highest conductivity) among other potential electrodes such as indium tin oxide (ITO), ionic PAAm hydrogel film, and PEDOT:PSS (Heraeus Deutschland GmbH & Co., Germany) [Fig. 1(e)]. In addition, the AC impedance of other materials varies significantly at different frequencies [Fig. 1(f)]. On the other hand, the impedance of the nanocomposite is maintained almost same and is extremely low (~8.5 Ω) over almost the entire frequency range.

The electrical properties of the alginate hydrogel-based nanocomposite can be affected by the type of conducting filler materials.[33] Therefore, AgNWs, carbon black (CB), multiwalled carbon nanotube (CNT),[34] and PEDOT:PSS were compared as conducting filler materials in Figs. 1(g) and 1(h). In the case of CNT, well-dispersed aqueous solution was used (0.3 mg/ml). The nanocomposite containing AgNWs exhibited the lowest resistance and AC impedance compared to the nanocomposites containing other conductive fillers. Finally, the influence of the AgNW concentration on the electrical properties of the nanocomposites was evaluated [Figs. 1(i) and 1(j)]. The resistance and AC impedance of the nanocomposites decreased with the increase in the AgNW concentration in the alginate hydrogel matrix.

Figure 2 shows the change in the electrical performance of the nanocomposites during stretching deformation. Nanocomposites with different concentrations of AgNWs were prepared [Fig. 2(a)], and stretching tests were performed in the strain range of 0–30% considering maximum stretchability of the human skin. The resistance of the nanocomposite

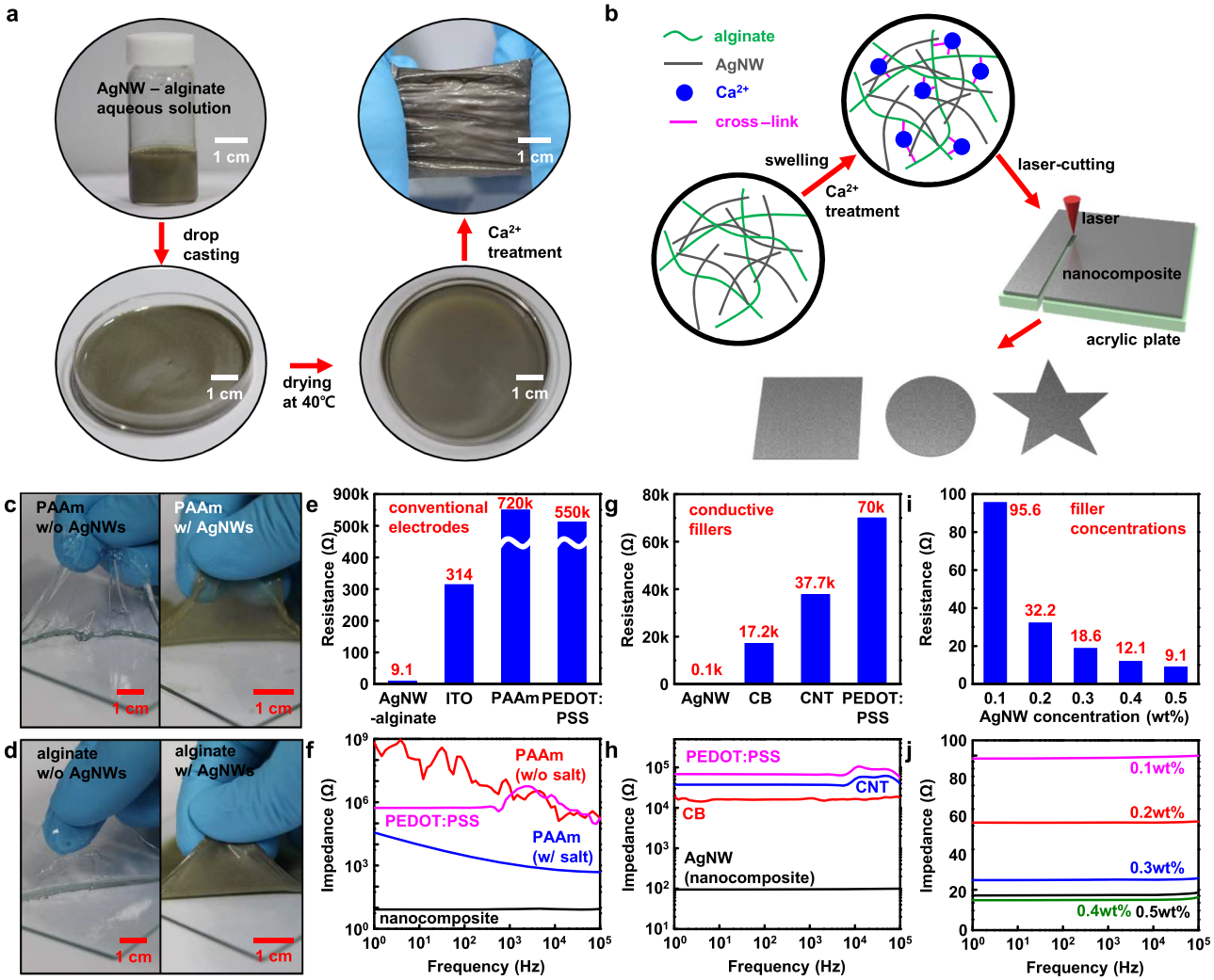

FIG. 1. (a) Fabrication process of the nanocomposite hydrogel electrode. (b) Illustration of the microstructure change during fabrication process and laser-cutting process for manufacturing of the nanocomposite. Images of (c) PAAm with and without AgNWs and (d) alginate hydrogel with and without AgNWs; the ratio of filler to the hydrogel matrix is 0.5 wt. %. Comparison of (e) resistance and (f) AC impedance among the nanocomposite and other conventional electrodes. Comparison of (g) resistance and (h) AC impedance among AgNW and other conductive fillers; the ratio of filler to the alginate matrix is 0.5 wt. % for AgNW and CB, 0.15 wt. % for CNT, and 7.5 wt. % for PEDOT:PSS. Comparison of (i) resistance and (j) AC impedance among nanocomposites with different AgNW concentrations (0.1–0.5 wt. %).

prepared with the AgNWs of the high concentration is not significantly affected by the applied strain [Fig. 2(b)]. However, resistance of the nanocomposite prepared with the AgNWs of the low concentration varies considerably depending on the applied strain. At first, the resistance increases sharply as the applied strain increases and subsequently fluctuates [Fig. 2(b)]. However, the resistance drops sharply when the strain is between 15% and 20%. After that, the resistance increases again as the strain increases. The same tendency is also found in the AC impedance measurement results [Fig. 2(c)]. Furthermore, the AC impedance monitoring data in the wide range of frequencies show the same tendency regardless of the frequency and AgNW concentrations [Figs. 2(d)–2(h)].

The sharp decrease in both resistance and AC impedance at the applied strain around 20% can be explained by the change of nanowire alignment inside the nanocomposite. To analyze the change, the nanocomposite is stretched from 0% to 30% [Fig. 2(i)], and a freeze-drying method was used to fix the shape of the nanowire network. Then the freeze-dried nanocomposite was observed by using a scanning electron microscope (SEM). In the SEM images [Fig. 2(j)], the AgNW network seems completely random initially. However, when the strain reaches 20%, the AgNWs rotate in the hydrogel media and are aligned following the stretching direction. This alignment of the nanowires in the viscous hydrogel media leads to the sharp decrease in the AC impedance and DC

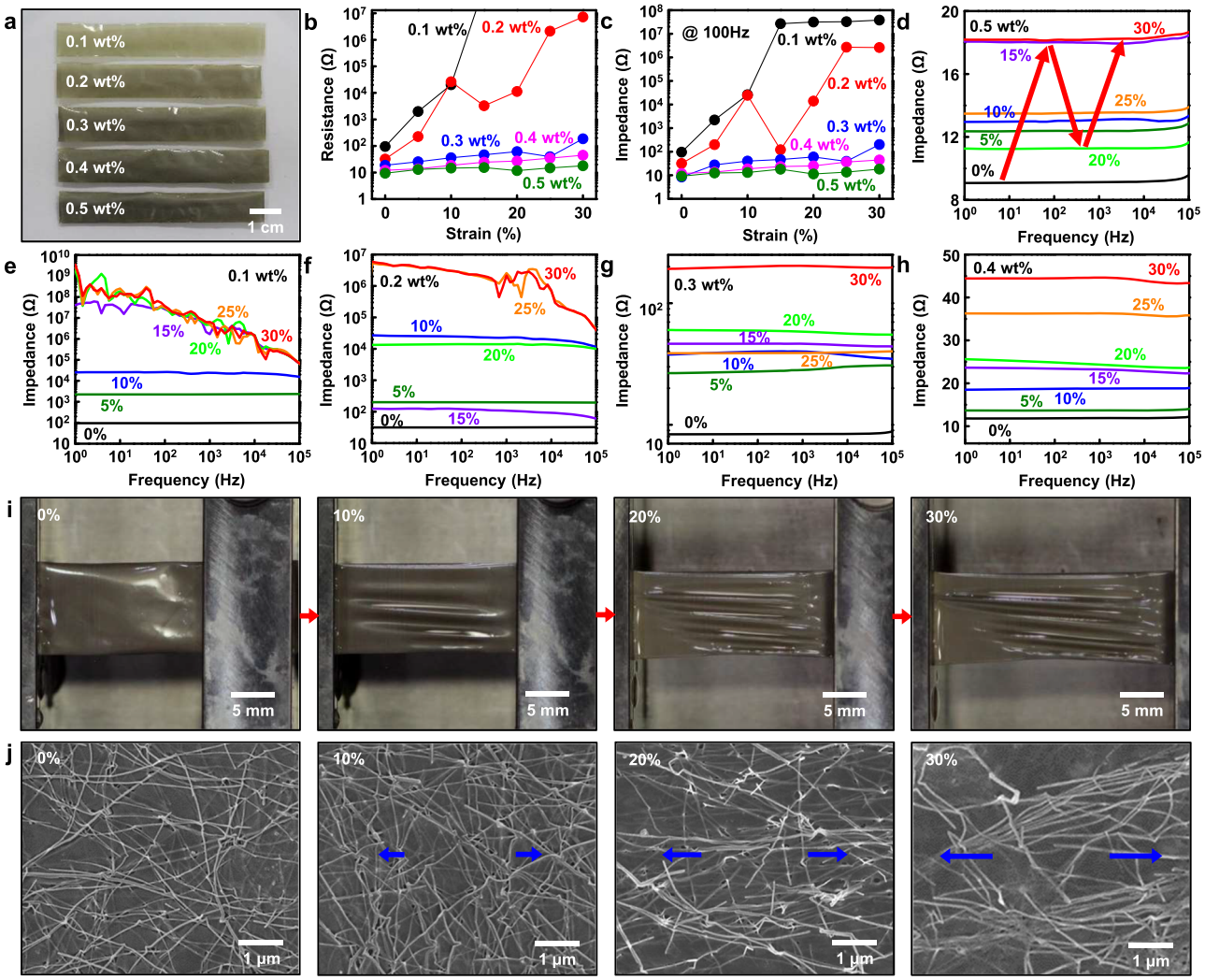

FIG. 2. (a) Image of nanocomposite electrodes with different concentrations of AgNW. (b) Resistance change of the nanocomposite electrodes with different AgNW concentrations during stretching test. (c) Change of AC impedance at 100 Hz of each nanocomposite electrodes during stretching test. AC impedance measurement of the nanocomposite electrode with (d) 0.5 wt. %, (e) 0.1 wt. %, (f) 0.2 wt. %, (g) 0.3 wt. %, and (h) 0.4 wt. % of AgNW during stretching test. (i) Images of the nanocomposite electrode during uniaxial stretching from 0% to 30%. (j) SEM images of the freeze-dried nanocomposite electrode during stretching from 0% to 30%.

resistance of the nanocomposite around 20% applied strain. Additional stretching induces the disconnections in the percolation network, resulting in the sharp increase of the resistance and AC impedance.

As the nanocomposite has high conductivity under both DC and AC modes, it can be applied to various types of electronic devices and/or energy storage devices. In such applications, the nanocomposite should be processed in various sizes and shapes. In this work, we used a laser cutting method to pattern the nanocomposite into desired shapes.[35] First, the nanocomposite film is placed on an acrylic supporting plate [Fig. 3(a)] and loaded onto the laser cutting machine (VLS 6.60, Universal Laser Systems Inc., United States). The film was wetted prior to the laser cutting process. This wet process does not degrade the electrical conductivity of the nanocomposite (Fig. S1). On the contrary, the laser cutting of the dried nanocomposite generated sparks, which could result in local burning of the nanocomposite. After the laser cutting process, the patterned nanocomposite can be transferred onto a variety of substrates including PAAm hydrogel films, polyethylene terephthalate films, and glass. Figure 3(b) shows the detailed images of each processing step.

The nanocomposite can be cut into any shape with a narrow width of 1 mm or more because the laser beam has a resolution in the order of hundreds of micrometers. Various examples including heart, four-leaf clover, human,

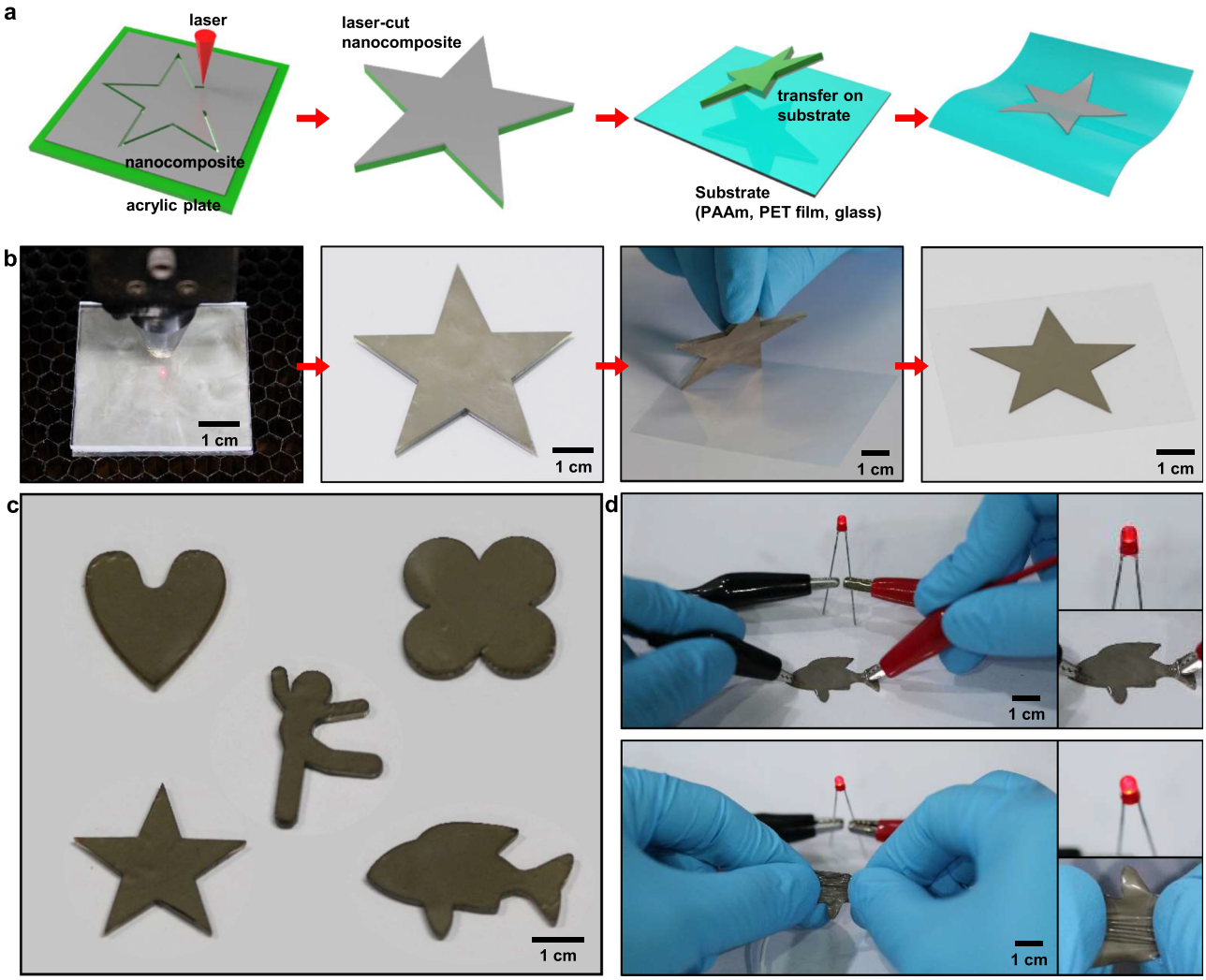

FIG. 3. (a) Illustration of procedures for nanocomposite processing using the laser-cutting machine. (b) Images for each step of nanocomposite processing procedure. (c) Various shapes of nanocomposites after the laser-cutting process. (d) Images of LED lights while current flows through nanocomposite before (upper images) and after stretching (lower images).

star, and fish-shaped nanocomposites are present in Fig. 3(c). The nanocomposite was cut into a shape of electric wires and various other objects, and they were integrated with light emitting diodes (LEDs), as shown in Fig. 3(d) (upper). The LED is turned on as the current passes through the nanocomposite, which is part of the electric circuit. While stretched, the fish-shaped nanocomposite maintains its high conductivity and the LED still remains turned on brightly [Fig. 3(d), lower]. This demonstration indicates that high electrical conductivity of the nanocomposite is not affected by the laser cutting process.

Young's modulus of the AgNW-alginate hydrogel nanocomposite was 15.5 MPa; therefore, they are not as soft as the human skin with a modulus of 0.05–0.15 MPa.[36] Nevertheless, the device-level softness can be further improved to be comparable to that of the human skin.[37] Integrating a low-modulus hydrogel layer to the hydrogel nanocomposite to form a bilayer structure can be a solution.[38] Figure 4(a) shows images of the nanocomposite attached on a PAAm hydrogel layer while it is stretched up to 100%. As the PAAm has a very low modulus of 0.008 MPa, the stress applied to the nanocomposite electrode layer is well dissipated and released away. The finite element method (FEM) analysis [Fig. 4(b)] shows the same tendency with the real stretching tests. Therefore, it can be inferred from the analysis that the nanocomposite can be reliably used on the stretched skin when integrated with the PAAm layer. Additional FEM analyses are performed when the nanocomposite electrode is

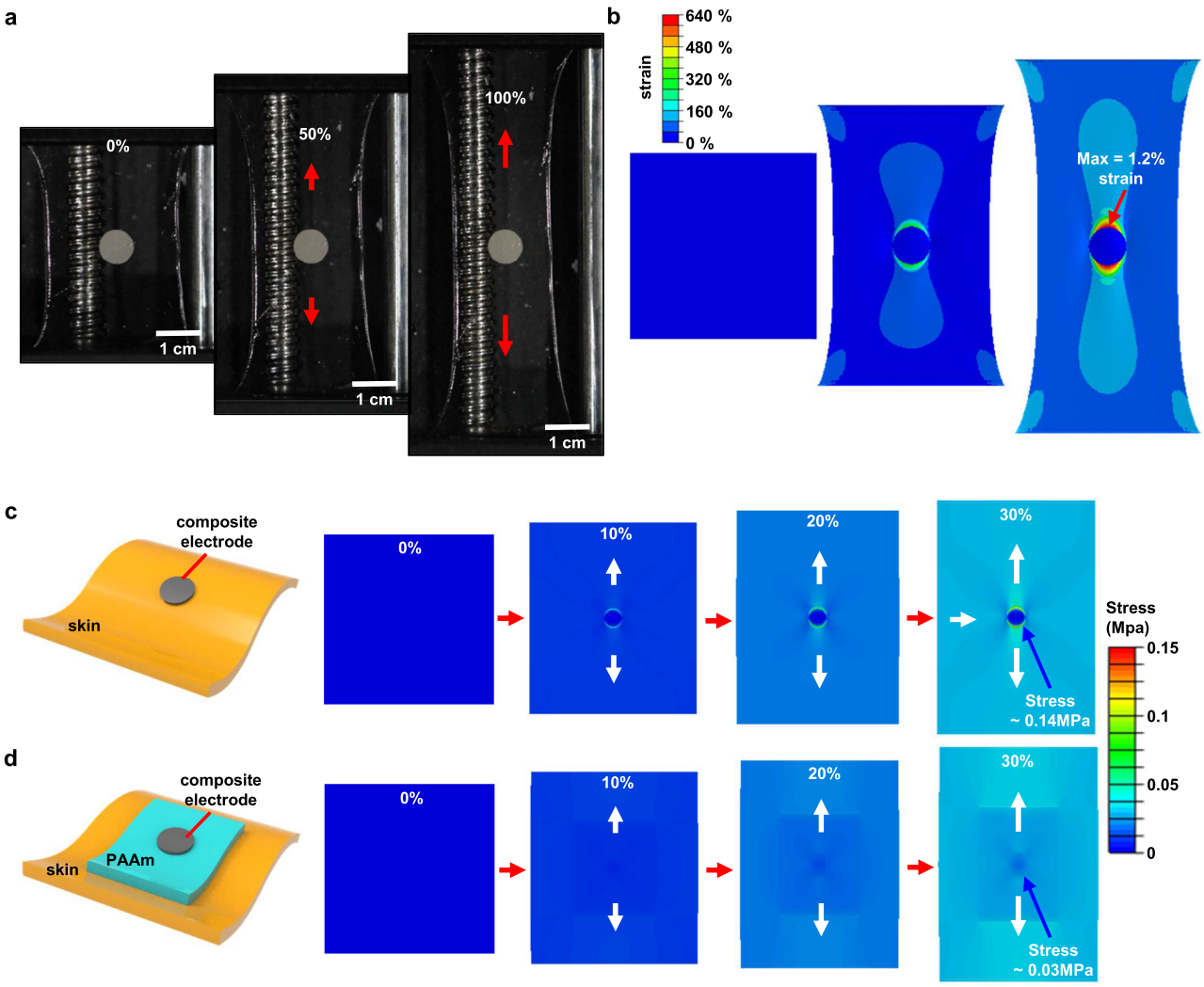

FIG. 4. (a) Stretching images of circular hydrogel composite attached onto the PAAm substrate. (b) FEM simulation images of predicted strain distribution near the composite electrode attached onto the PAAm substrate. (c) Illustration of hydrogel composite on the skin and FEM simulation images of predicted stress distribution on the skin when the overall system is stretched up to 30%. (d) Illustration of hydrogel composite on the skin with the PAAm layer in between, and FEM simulation images of predicted stress distribution on the skin when the overall system is stretched up to 30%.

placed directly on the skin and when the PAAm layer is placed between the electrode and the skin. The FEM analysis results show that a stress of 0.14 MPa acts on the skin when the skin is stretched up to 30% [Fig. 4(c)]. On the other hand, a stress of only 0.04 MPa acts on the skin when the PAAm layer is placed between the nanocomposite electrode and the skin [Fig. 4(d)]. The analysis reveals that integration of the low modulus PAAm hydrogel with the AgNW-alginate nanocomposite electrode causes less stress on the skin, which consequently creates a better interface with comfortable feeling.

The detailed explanation for the FEM analysis is described as follows. For the stretching simulation, the disk-shaped nanocomposite (diameter: 6.0 mm, thickness: 0.06 mm) was placed on the PAAm hydrogel layer (size: $30 \times 30 \times 1.0$ mm^3) and discretized with eight-node hexahedral solid elements. The perfect bonding was assumed between the layers, and the boundary conditions corresponding to the 100% stretching were applied on the hydrogel layer. For the stretching simulation on the skin substrate, either the nanocomposite electrode alone or the hydrogel layer with the nanocomposite was placed on the skin substrate (size: $60 \times 60 \times 0.5$ mm^3) and the boundary conditions corresponding to the 30% stretching were applied on the skin substrate. The incompressible neo-Hookean model was used to represent the behavior of the nanocomposite, PAAm layer, and the skin substrate,

$$W = C_1(I_1 - 3),$$

where W is the strain energy potential, I_1 is the first invariant of the left Cauchy-Green tensor, and C_1 is a material parameter (2.65 MPa for the nanocomposite, 2.03 kPa for PAAm, and 16.7 kPa for skin). Tensile tests were performed with a universal testing machine (Instron-5543, Instron corp., United States), and Young's moduli were calculated from the stress-strain curves.

The nanocomposite in combination with the soft PAAm layer can be used to make high-performance stretchable electrodes for various wearable devices.[39,40] An example of such a wearable device is the wearable antenna,[41] which is an essential component in wireless communication of mobile wearable electronics.[42] For an efficient data and energy transfer,[43] the overall resistance of the antenna should be low, while it should make a conformal integration with the human skin[44] to minimize unwanted noise generation due to body movements. For example, the communication efficiency through the wearable antenna changes significantly even with very small vibrations of the skin. The inductive coil is a basic component of the wearable antenna [Fig. 5(a)].[45] In wireless communication,[46] data are sent and received via radio frequency waves. The antenna has a specific resonant frequency at which the efficiency of data transmission is maximized.[47] This resonance frequency can be found by analyzing the S-parameters, particularly the S_{11} value when data communication is performed with a single electrode system. S_{11} analysis provides important

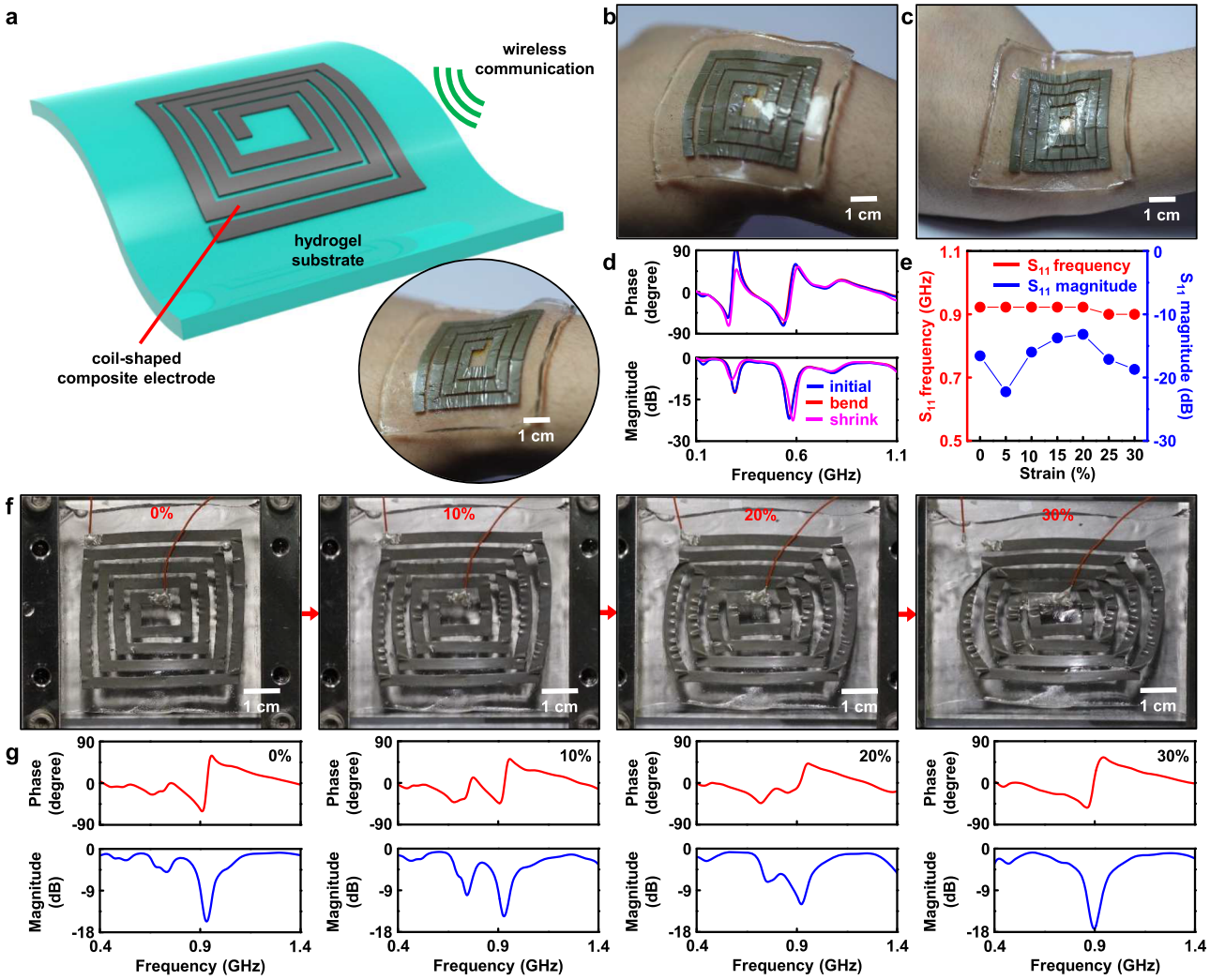

FIG. 5. (a) Illustration of coil-shaped hydrogel composite electrode as a wearable antenna for wireless communication and its image (inset) when attached on the skin. Images of wearable antenna on the skin while (b) outward and (c) inward bending. (d) S_{11} peak frequency and magnitude values during each deformation. (e) S_{11} peak analysis data during stretching up to 30%. (f) Images of the uniaxially stretched hydrogel composite antenna attached on the PAAm substrate. (g) S_{11} analysis data of the wearable antenna for each stretching state from 0% to 30%.

information on how much data the antenna can receive with respect to the overall magnitude of the signals.

The antenna was fabricated by patterning the nanocomposite with a laser cutting method and integrating it on a PAAm hydrogel layer [inset of Fig. 5(a)]. The antenna attached on the skin showed reliable performance even after deformation such as outward [Fig. 5(b)] and inward bending [Fig. 5(c)] owing to the soft PAAm layer. While the antenna was deformed on the skin, the frequency and magnitude of the S_{11} peak were measured [Fig. 5(d)]. Although the S_{11} magnitude value fluctuates while the antenna is deformed, the resonant frequency remains almost same. Similarly, S_{11} was also measured while the antenna was stretched from 0% to 30%, and the results are summarized in Fig. 5(e). As in the case of bending, the resonance frequency was maintained almost constant, while the S_{11} magnitude slightly fluctuated. As the resonance frequency always exists within the frequency range of the S_{11} peaks, the signal loss is not significant, even though the antenna is stretched on the skin. The resonance frequency of a stretchable antenna prepared with a highly conducting rubber can be dramatically changed by the applied strain when the conducting rubber is patterned into a line shape.[48] Moreover, the stretching deformation of a circular- or rectangular-shaped stretchable antenna leads to a resonance frequency shift of the stretchable antenna.[49] Therefore, the excellent

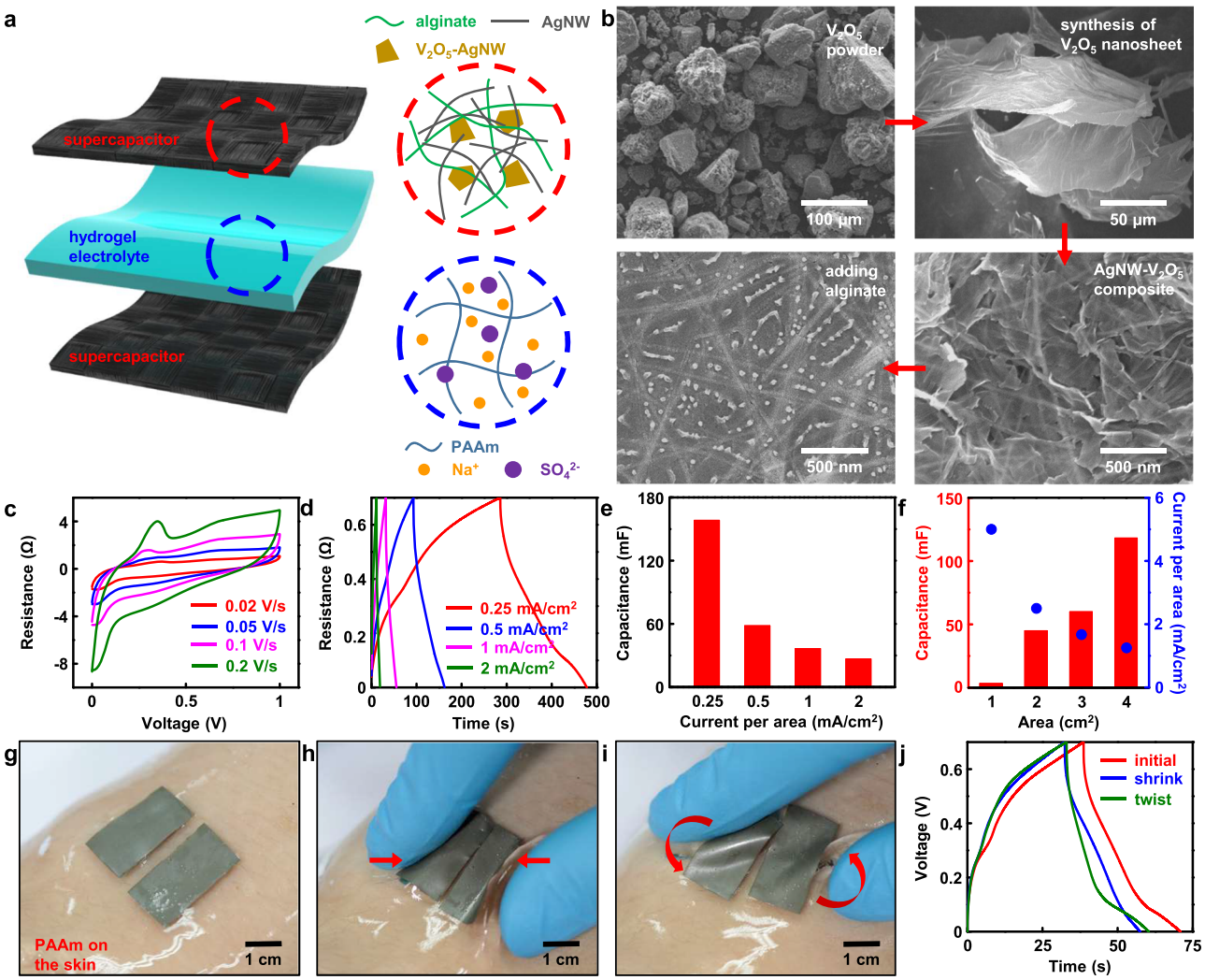

FIG. 6. (a) Illustration of the overall supercapacitors composed of the hydrogel composite (containing V_2O_5 nanosheets) and PAAm electrolyte layer (containing 1M Na_2SO_4). (b) SEM images that describe the preparation steps of V_2O_5 nanosheet and supercapacitor active layer. (c) CV curves of the supercapacitor under different scanning rates. (d) Galvanostatic charge-discharge curve under different areal current densities. (e) Calculated capacitance of the supercapacitor under each level of areal current density. (f) Capacitance change with respect to the increase in the size of the supercapacitor. Images of the supercapacitors attached on the skin with the PAAm layer in between during (g) initial, (h) crumpling, and (i) twisting state. (j) Galvanostatic charge-discharge curves under each deformation state.

stability of the stretchable antenna demonstrated here is mainly attributed to the presence of the integrated PAAm hydrogel layer between the stretchable antenna and the human skin. In addition, stretching images of the antenna and each raw data of S_{11} analysis are shown in Figs. 5(f) and 5(g), respectively.

As another demonstration of wearable devices,[50] a skin-mountable supercapacitor was developed. For energy storage devices such as supercapacitors,[51] electrodes with high conductivity are essential for efficient current collection.[52] Usually, active materials for redox reactions are coated on the current collector.[53] However, instead of the conventional design of supercapacitors,[54] an all-in-one type supercapacitor in which the active material and the current collector are prepared as a single layer was developed in this study [Fig. 6(a)]. As shown in SEM images [Fig. 6(b)], V_2O_5 nanosheets were first synthesized from the V_2O_5 powder,[55] and 50 mg of V_2O_5 nanosheets were dispersed in 10 g of water with tip sonication. The V_2O_5 aqueous suspension was then mixed with 10 ml of 0.5 wt. % AgNW aqueous suspension, resulting in the formation of a AgNW-V_2O_5 mixture after 12 h. The mixed solution containing the AgNW-V_2O_5 mixture was centrifuged at 2000 rpm for 5 min, and the supernatant was collected to mix with 20 ml of AgNW aqueous suspension. Subsequently, 0.6 g of sodium alginate was dissolved in the mixed solution by stirring at 70 °C on a hot plate, and 0.5 g of the resulting solution was poured onto a glass substrate with an area of 7 cm^2. The poured solution was dried at 40 °C and treated with 0.1M $CaCl_2$ aqueous solution for 20 min. The resulting film containing the active material maintains the high electrical conductivity of the original AgNW-alginate hydrogel nanocomposite electrode, thus enabling the fabrication of electrochemically active electrodes for the all-in-one type supercapacitor.

The prepared electrode and a pseudo-solid-state electrolyte film of the PAAm hydrogel containing 1M Na_2SO_4 were stacked together for the supercapacitor assembly. A cyclic voltammetry (CV) analysis and a galvanostatic charge-discharge test were performed under various scan rates [Fig. 6(c)] and current densities [Fig. 6(d)]. The V_2O_5 nanosheets are a pseudo-capacitive material. Therefore, the supercapacitor electrode with the V_2O_5 nanosheet electrode shows a different shape of the CV curve as compared to a typical electrical double layered capacitor exhibiting a rectangular CV curve. Several peaks related to the reduction and oxidation of the V_2O_5 nanosheets during the charging/discharging are clearly observed, as shown in Fig. 6(c). Several inflection points observed in the galvanostatic charge-discharge curves also indicates redox reactions of the V_2O_5 nanosheets [Fig. 6(d)]. The galvanostatic charge-discharge data show that the capacitance of the supercapacitors sharply decreases from 158.33 to 26.67 mF as the areal current density increases from 0.25 to 2 mA/cm^2 [Fig. 6(e)]. In addition, the capacitance of the supercapacitors increases sharply as the area increases when charging and discharging under 5 mA [Fig. 6(f)]. This is because the areal current density decreases as the area increases. When attached on the skin with the PAAm substrate, the supercapacitors can be deformed by crumpling and twisting along the counterclockwise direction [Figs. 6(g)–6(i)]. Although the supercapacitors themselves bend while deforming on the skin, the galvanostatic charge-discharge tests show that the change in the capacitance values is negligible [Fig. 6(j)].

In summary, a highly conductive hydrogel nanocomposite was developed using the alginate hydrogel and AgNWs. The nanocomposite maintains a low AC impedance over a wide frequency range and shows low resistance under the DC mode. The laser cutting method could pattern the nanocomposite into various desired shapes. The decreased softness due to the addition of the AgNWs could be improved by integrating the soft PAAm hydrogel substrate, which helped release the induced stress. By combining the high electrical conductivity of the nanocomposite and the stress release property of the soft PAAm substrate, the nanocomposite could be used for the fabrication of a wearable antenna and a supercapacitor. The conformal integration of soft nanocomposite-based devices with the human skin enabled reliable operation of wearable devices.[56] For example, the resonance frequency of the wearable antenna was not affected by mechanical deformation such as outward and inward bending, ensuring an efficient data and energy transfer[57] to wearable devices[58] integrated with a wearable antenna. A mechanically flexible all-in-one type supercapacitor was successfully fabricated by functionalizing the nanocomposite with V_2O_5 nanosheets, which functioned well even under mechanical deformations. The AgNW-alginate nanocomposite[59] electrode provides a meaningful solution for soft electrodes in wearable electronics.

See supplementary material for a movie file to show the inhomogeneity of PAAm hydrogel cured in the presence of AgNWs and resistance data to compare the electrical conductivity of the composite film by normal cutting and laser cutting.

This work was supported by the Institute for Basic Science (Grant No. IBS-R006-A1). J.H.K. acknowledges the Basic Science Research Program through the National Research Foundation of Korea (NRF) funded by the Ministry of Science, ICT and Future Planning (Grant No. 2015R1C1A1A01051620). The authors thank the staff of the Research Institute of Advanced Materials (RIAM).

REFERENCES

[1] Y.-J. Liu, W.-T. Cao, M.-G. Ma, and P. Wan, ACS Appl. Mater. Interfaces **9**(30), 25559 (2017).
[2] X. Jing, H.-Y. Mi, Y.-J. Lin, E. Enriquez, X.-F. Peng, and L.-S. Turng, ACS Appl. Mater. Interfaces **10**(24), 20897 (2018).
[3] C.-C. Kim, H.-H. Lee, K. H. Oh, and J.-Y. Sun, Science **353**(6300), 682 (2016).
[4] E. P. Gilshteyn, D. Amanbayev, A. S. Anisimov, T. Kallio, and A. G. Nasibulin, Sci. Rep. **7**(1), 17449 (2017).
[5] L. Zhong, Y. Lu, H. Li, Z. Tao, and J. Chen, ACS Sustainable Chem. Eng. **6**(6), 7761 (2018).

[6]Z. Chen, J. W. F. To, C. Wang, Z. Lu, N. Liu, A. Chortos, L. Pan, F. Wei, Y. Cui, and Z. Bao, Adv. Energy Mater. **4**(12), 1400207 (2014).
[7]J.-K. Song, D. Son, J. Kim, Y. J. Yoo, G. J. Lee, L. Wang, M. K. Choi, J. Yang, M. Lee, K. Do, J. H. Koo, N. Lu, J. H. Kim, T. Hyeon, Y. M. Song, and D.-H. Kim, Adv. Funct. Mater. **27**(6), 1605286 (2017).
[8]M. M. Puurtinen, S. M. Komulainen, P. K. Kauppinen, J. A. V. Malmivuo, and J. A. K. Hyttinen, presented at the 2006 Conference Proceedings of the IEEE Engineering in Medicine and Biology Society, 2006.
[9]S. L. Swisher, M. C. Lin, A. Liao, E. J. Leeflang, Y. Khan, F. J. Pavinatto, K. Mann, A. Naujokas, D. Young, S. Roy, M. R. Harrison, A. C. Arias, V. Subramanian, and M. M. Maharbiz, Nat. Commun. **6**, 6575 (2015).
[10]H. Lee, T. K. Choi, Y. B. Lee, H. R. Cho, R. Ghaffari, L. Wang, H. J. Choi, T. D. Chung, N. Lu, T. Hyeon, S. H. Choi, and D.-H. Kim, Nat. Nanotechnol. **11**, 566 (2016).
[11]S. H. Kim, S. Jung, I. S. Yoon, C. Lee, Y. Oh, and J.-M. Hong, Adv. Mater. **30**(26), 1800109 (2018).
[12]D. Wirthl, R. Pichler, M. Drack, G. Kettlguber, R. Moser, R. Gerstmayr, F. Hartmann, E. Bradt, R. Kaltseis, C. M. Siket, S. E. Schausberger, S. Hild, S. Bauer, and M. Kaltenbrunner, Sci. Adv. **3**(6), e1700053 (2017).
[13]J. Hur, K. Im, S. W. Kim, J. Kim, D.-Y. Chung, T.-H. Kim, K. H. Jo, J. H. Hahn, Z. Bao, S. Hwang, and N. Park, ACS Nano **8**(10), 10066 (2014).
[14]V. R. Feig, H. Tran, M. Lee, and Z. Bao, Nat. Commun. **9**(1), 2740 (2018).
[15]L. Pan, G. Yu, D. Zhai, H. R. Lee, W. Zhao, N. Liu, H. Wang, B. C.-K. Tee, Y. Shi, Y. Cui, and Z. Bao, Proc. Natl. Acad. Sci. U. S. A. **109**(24), 9287 (2012).
[16]C. Kleber, M. Bruns, K. Lienkamp, J. Rühe, and M. Asplund, Acta Biomater. **58**, 365 (2017).
[17]A. J. Patton, R. A. Green, and L. A. Poole-Warren, APL Mater. **3**(1), 014912 (2015).
[18]J. Kim, D. Son, M. Lee, C. Song, J.-K. Song, J. H. Koo, D. J. Lee, H. J. Shim, J. H. Kim, M. Lee, T. Hyeon, and D.-H. Kim, Sci. Adv. **2**(1), e1501101 (2016).
[19]J. Park, S. Choi, A. H. Janardhan, S.-Y. Lee, S. Raut, J. Soares, K. Shin, S. Yang, C. Lee, K.-W. Kang, H. R. Cho, S. J. Kim, P. Seo, W. Hyun, S. Jung, H.-J. Lee, N. Lee, S. H. Choi, M. Sacks, N. Lu, M. E. Josephson, T. Hyeon, D.-H. Kim, and H. J. Hwang, Sci. Transl. Med. **8**(344), 344ra86 (2016).
[20]S. Kabiri Ameri, R. Ho, H. Jang, L. Tao, Y. Wang, L. Wang, D. M. Schnyer, D. Akinwande, and N. Lu, ACS Nano **11**(8), 7634 (2017).
[21]M. K. Choi, I. Park, D. C. Kim, E. Joh, O. K. Park, J. Kim, M. Kim, C. Choi, J. Yang, K. W. Cho, J.-H. Hwang, J.-M. Nam, T. Hyeon, J. H. Kim, and D.-H. Kim, Adv. Funct. Mater. **25**(46), 7109 (2015).
[22]C. Zhan, G. Yu, Y. Lu, L. Wang, E. Wujcik, and S. Wei, J. Mater. Chem. C **5**(7), 1569 (2017).
[23]S. Lim, D. Son, J. Kim, Y. B. Lee, J.-K. Song, S. Choi, D. J. Lee, J. H. Kim, M. Lee, T. Hyeon, and D.-H. Kim, Adv. Funct. Mater. **25**(3), 375 (2015).
[24]P. Thoniyot, M. J. Tan, A. A. Karim, D. J. Young, and X. J. Loh, Adv. Sci. **2**(1-2), 1400010 (2015).
[25]V. Pardo-Yissar, R. Gabai, A. N. Shipway, T. Bourenko, and I. Willner, Adv. Mater. **13**(17), 1320 (2001).
[26]C. Wang, N. T. Flynn, and R. Langer, Adv. Mater. **16**(13), 1074 (2004).
[27]Y. Gao, J. Song, S. Li, C. Elowsky, Y. Zhou, S. Ducharme, Y. M. Chen, Q. Zhou, and L. Tan, Nat. Commun. **7**, 12316 (2016).
[28]S. Choi, S. I. Han, D. Jung, H. J. Hwang, C. Lim, S. Bae, O. K. Park, C. M. Tschabrunn, M. Lee, S. Y. Bae, J. W. Yu, J. H. Ryu, S.-W. Lee, K. Park, P. M. Kang, W. B. Lee, R. Nezafat, T. Hyeon, and D.-H. Kim, Nat. Nanotechnol. **13**(11), 1048 (2018).
[29]S. Choi, J. Park, W. Hyun, J. Kim, J. Kim, Y. B. Lee, C. Song, H. J. Hwang, J. H. Kim, T. Hyeon, and D.-H. Kim, ACS Nano **9**(6), 6626 (2015).
[30]S. Lin, C. Cao, Q. Wang, M. Gonzalez, J. E. Dolbow, and X. Zhao, Soft Matter **10**(38), 7519 (2014).
[31]C. Choi, M. K. Choi, S. Liu, M. S. Kim, O. K. Park, C. Im, J. Kim, X. Qin, G. J. Lee, K. W. Cho, M. Kim, E. Joh, J. Lee, D. Son, S.-H. Kwon, N. L. Jeon, Y. M. Song, N. Lu, and D.-H. Kim, Nat. Commun. **8**(1), 1664 (2017).
[32]Y. Yanagisawa, Y. Nan, K. Okuro, and T. Aida, Science **359**(6371), 72 (2018).
[33]S. Jung, J. H. Kim, J. Kim, S. Choi, J. Lee, I. Park, T. Hyeon, and D.-H. Kim, Adv. Mater. **26**(28), 4825 (2014).
[34]J. H. Koo, S. Jeong, H. J. Shim, D. Son, J. Kim, D. C. Kim, S. Choi, J.-I. Hong, and D.-H. Kim, ACS Nano **11**(10), 10032 (2017).
[35]C. Keplinger, J.-Y. Sun, C. C. Foo, P. Rothemund, G. M. Whitesides, and Z. Suo, Science **341**(6149), 984 (2013).
[36]M. Pawlaczyk, M. Lelonkiewicz, and M. Wieczorowski, Adv. Dermatol. Allergol. **5**, 302 (2013).
[37]S. K. Ameri, M. Kim, I. A. Kuang, W. K. Perera, M. Alshiekh, H. Jeong, U. Topcu, D. Akinwande, and N. Lu, npj 2D Mater. Appl. **2**(1), 19 (2018).
[38]Y. Tingting, Z. Yujia, T. Dashuai, L. Xinming, Z. Xiaobei, L. Shuyuan, J. Xin, L. Zhihong, and Z. Hongwei, 2D Mater. **4**(3), 035020 (2017).
[39]S. Hong, J. Lee, K. Do, M. Lee, J. H. Kim, S. Lee, and D.-H. Kim, Adv. Funct. Mater. **27**(48), 1704353 (2017).
[40]S. R. Madhvapathy, Y. Ma, M. Patel, S. Krishnan, C. Wei, Y. Li, S. Xu, X. Feng, Y. Huang, and J. A. Rogers, Adv. Funct. Mater. **28**(34), 1802083 (2018).
[41]D. Son, J. Lee, D. J. Lee, R. Ghaffari, S. Yun, S. J. Kim, J. E. Lee, H. R. Cho, S. Yoon, S. Yang, S. Lee, S. Qiao, D. Ling, S. Shin, J.-K. Song, J. Kim, T. Kim, H. Lee, J. Kim, M. Soh, N. Lee, C. S. Hwang, S. Nam, N. Lu, T. Hyeon, S. H. Choi, and D.-H. Kim, ACS Nano **9**(6), 5937 (2015).
[42]Z. Yan, T. Pan, G. Yao, F. Liao, Z. Huang, H. Zhang, M. Gao, Y. Zhang, and Y. Lin, Sci. Rep. **7**, 42227 (2017).
[43]J. Lee, B. Yoo, H. Lee, G. D. Cha, H.-S. Lee, Y. Cho, S. Y. Kim, H. Seo, W. Lee, D. Son, M. Kang, H. M. Kim, Y. I. Park, T. Hyeon, and D.-H. Kim, Adv. Mater. **29**(1), 1603169 (2017).
[44]J. Kang, D. Son, G.-J. N. Wang, Y. Liu, J. Lopez, Y. Kim, J. Y. Oh, T. Katsumata, J. Mun, Y. Lee, L. Jin, J. B.-H. Tok, and Z. Bao, Adv. Mater. **30**(13), 1706846 (2018).
[45]B. Zhan, D. Su, S. Liu, and F. Liu, AIP Adv. **7**(6), 065313 (2017).
[46]L. Lu, P. Gutruf, L. Xia, D. L. Bhatti, X. Wang, A. Vazquez-Guardado, X. Ning, X. Shen, T. Sang, R. Ma, G. Pakeltis, G. Sobczak, H. Zhang, D.-o. Seo, M. Xue, L. Yin, D. Chanda, X. Sheng, M. R. Bruchas, and J. A. Rogers, Proc. Natl. Acad. Sci. U. S. A. **115**(7), E1374 (2018).
[47]J. Kim, R. Ghaffari, and D.-H. Kim, Nat. Biomed. Eng. **1**, 0049 (2017).
[48]M. Park, J. Im, M. Shin, Y. Min, J. Park, H. Cho, S. Park, M.-B. Shim, S. Jeon, D.-Y. Chung, J. Bae, J. Park, U. Jeong, and K. Kim, Nat. Nanotechnol. **7**, 803 (2012).
[49]J. Kim, A. Banks, H. Cheng, Z. Xie, S. Xu, K.-I. Jang, J. W. Lee, Z. Liu, P. Gutruf, X. Huang, P. Wei, F. Liu, K. Li, M. Dalal, R. Ghaffari, X. Feng, Y. Huang, S. Gupta, U. Paik, and J. A. Rogers, Small **11**(8), 906 (2015).
[50]D. Son, J. Kang, O. Vardoulis, Y. Kim, N. Matsuhisa, J. Y. Oh, J. W. F. To, J. Mun, T. Katsumata, Y. Liu, A. F. McGuire, M. Krason, F. Molina-Lopez, J. Ham, U. Kraft, Y. Lee, Y. Yun, J. B. H. Tok, and Z. Bao, Nat. Nanotechnol. **13**(11), 1057 (2018).
[51]S. Jung, J. Lee, T. Hyeon, M. Lee, and D.-H. Kim, Adv. Mater. **26**(36), 6329 (2014).
[52]X. Wang, C. Yang, J. Jin, X. Li, Q. Cheng, and G. Wang, J. Mater. Chem. A **6**(10), 4432 (2018).
[53]D. Qi, Y. Liu, Z. Liu, L. Zhang, and X. Chen, Adv. Mater. **29**(5), 1602802 (2017).
[54]Z. Lv, Y. Luo, Y. Tang, J. Wei, Z. Zhu, X. Zhou, W. Li, Y. Zeng, W. Zhang, Y. Zhang, D. Qi, S. Pan, X. J. Loh, and X. Chen, Adv. Mater. **30**(2), 1704531 (2018).
[55]J. Zhu, L. Cao, Y. Wu, Y. Gong, Z. Liu, H. E. Hoster, Y. Zhang, S. Zhang, S. Yang, Q. Yan, P. M. Ajayan, and R. Vajtai, Nano Lett. **13**(11), 5408 (2013).
[56]D. Son, S. I. Chae, M. Kim, M. K. Choi, J. Yang, K. Park, V. S. Kale, J. H. Koo, C. Choi, M. Lee, J. H. Kim, T. Hyeon, and D.-H. Kim, Adv. Mater. **28**(42), 9326 (2016).
[57]L. Y. Chen, B. C. K. Tee, A. L. Chortos, G. Schwartz, V. Tse, D. J. Lipomi, H. S. P. Wong, M. V. McConnell, and Z. Bao, Nat. Commun. **5**, 5028 (2014).
[58]J. Kim, H. J. Shim, J. Yang, M. K. Choi, D. C. Kim, J. Kim, T. Hyeon, and D.-H. Kim, Adv. Mater. **29**(38), 1700217 (2017).
[59]J. Guo, K. Zhao, X. Zhang, Z. Cai, M. Chen, C. Tian, and W. Junfu, Mater. Lett. **157**, 112 (2015).